A statistical framework for defining synergistic anticancer drug interactions

Diogo Dias[1,2,3,4], John Zobolas[5,6], Aleksandr Ianevski[1,2] and Tero Aittokallio[1,2,5,6,*]

[1]Institute for Molecular Medicine Finland (FIMM), HiLIFE, University of Helsinki, Helsinki, Finland
[2]iCAN Digital Precision Cancer Medicine Flagship, University of Helsinki and Helsinki University Hospital, Finland
[3]Hematology Research Unit Helsinki, University of Helsinki and Helsinki University Hospital Comprehensive Cancer Center, Helsinki, Finland
[4]Translational Immunology Research Program and Department of Clinical Chemistry and Hematology, University of Helsinki, Helsinki, Finland
[5]Institute for Cancer Research, Department of Cancer Genetics, Oslo University Hospital, Oslo, Norway
[6]Oslo Centre for Biostatistics and Epidemiology (OCBE), Faculty of Medicine, University of Oslo, Oslo, Norway
*Correspondence: Tero Aittokallio, PhD, Institute for Molecular Medicine Finland, FIMM, P.O. Box 20 (Tukholmankatu 8), FI-00014 University of Helsinki, Helsinki, Finland. Tel: +358 50 3182426, Email: tero.aittokallio@helsinki.fi

Abstract

Synergistic drug combinations have the potential to delay drug resistance and improve clinical outcomes in patients with advanced cancers. However, current cell-based screens lack robust statistical assessment to identify significant synergistic interactions for downstream experimental or clinical validation. Leveraging a large-scale dataset that systematically evaluated more than 2,000 drug combinations across 125 pan-cancer cell lines, we established reference null distributions separately for various synergy metrics and cancer types. These data-driven reference distributions enable estimation of empirical *p*-values to assess the significance of observed drug combination effects, thereby standardizing synergy detection in future studies. The statistical evaluation confirmed key synergistic combinations and uncovered novel combination effects that met stringent statistical criteria, yet were overlooked in the original analyses. We revealed cell context-specific drug combination effects across the tissue types and differences in statistical behavior of the synergy metrics. To demonstrate the general applicability of our approach to smaller-scale studies, we applied the reference distributions to evaluate the significance of combination effects in an independent dataset. We provide a fast and statistically rigorous approach to detecting synergistic drug interactions in new combinatorial screens, thereby supporting more standardized drug combination discovery.

Keywords: Drug combinations, High-throughput screening, Synergy scoring, Reference distributions, Empirical p-values, Statistical hypothesis testing

Introduction

Drug resistance in cancer renders most monotherapies eventually ineffective, leaving patients with relapsed or refractory disease in need of alternative treatment regimens, such as synergistic drug combinations that can overcome resistance mechanisms and improve clinical outcomes [1,2]. Synergistic combination therapies offer several clinical benefits, including enhanced efficacy, reduced likelihood of resistance, and lower toxicities through dose reduction [3].

High-throughput drug combination screening in disease models (cell lines, patient-derived cells, and organoids) has become a standard approach for identifying synergistic drug interactions effects in complex diseases [4-6]. Several anticancer screening studies have evaluated thousands of compound combinations in cancer cell lines and patient-derived cells to assess their co-inhibition effect on cell viability across increasing dose ranges [7-11]. However, even with high-throughput screening (HTS) automation, systematic evaluation of thousands of drug pairs across multiple cellular backgrounds with sufficient replicates becomes rapidly infeasible [8,11]. Furthermore, the scarcity of patient-derived cells further limits the number of combinations that can be evaluated in personalized medicine studies [12]. This results in moderate-sized datasets, where selected drug combinations are tested only in few cell models and doses, often without replicates [7,9,11-14].

The current challenge in combination therapeutic discovery is not generating phenotypic drug interaction data, but distinguishing genuine drug combination synergy from experimental noise. To quantify synergistic effect of the tested combinations, researchers typically rely on established synergy models and software tools, such as SynergyFinder [15] or Combenefit [16], which implement widely used synergy metrics, including Bliss independence [17], Loewe additivity [18], highest single-agent (HSA) [19,20], and zero interaction potency (ZIP) [21]. Despite decades of phenotypic drug combination testing, no standardized approach exists for defining drug combination synergy. Instead, researchers use various statistical and non-statistical approaches [7,11,22-25], which reduces consistency between screening studies, and delays the discovery of truly synergistic drug combinations for therapeutic applications [26]. For instance, arbitrary cutoffs, such as excess over Bliss > 10, can lead to different detection levels between studies [19,23]. These effect-size measures alone cannot determine whether the observed synergy levels are due to statistically significant interactions or random experimental fluctuations. While bootstrapping procedures can provide confidence intervals and empirical *p*-values [27], they rely heavily on the representativeness of the data, often producing biased estimates in small-scale datasets.

These challenges stem from a fundamental gap: researchers lack statistical benchmarks to distinguish true biological synergy effects from random experimental variation. Establishing such benchmarks requires comprehensive reference data from unbiased drug combinations – essentially, a reference null distribution that captures the background variability of synergy metrics under independent drug action. While generating such reference distributions exceeds the resources of most academic laboratories, the Sanger Institute systematically evaluated 2,025 combinations in 51 breast, 45 colorectal, and 29 pancreatic cancer cell lines [13]. These combinations were selected without prior knowledge of potential synergy or antagonism, hence

providing a sufficiently large, near-random set of combinations for unbiased statistical evaluation of observed synergy in other studies.

We developed a computational pipeline to leverage these unique data from the Sanger Institute to establish a statistically rigorous framework for defining drug combination synergy. Our approach predicts full dose-combination matrices from sparse experimental data, computes synergy scores using established synergy metrics, and generates tissue-specific reference distributions that enable empirical *p*-value estimation for any observed synergy metric. This approach transforms arbitrarily chosen effect-size thresholds into objective statistical assessments, providing publicly available reference distributions that allow researchers to calculate empirical *p*-values for their own combination experiments. Our framework addresses a fundamental gap in combination therapeutics by establishing the statistical foundation needed to accelerate reliable synergistic combination discovery, biological validation and clinical translation.

Results

Reference null distributions for statistical evaluation of drug interaction effects

To overcome the experimental and computational challenges of identifying statistically significant synergistic drug combinations, we developed a computational pipeline that integrates machine learning-based dose-combination effect prediction, synergy quantification, and statistical evaluation through reference null hypothesis distributions (**Fig. 1**). The approach is scalable and statistically robust across diverse drug classes, targets, and tissue contexts.

We applied the pipeline to the combination data described by Jaaks et al. [13], which tested 2,025 drug pairs across 125 cancer cell lines as part of the Genomics of Drug Sensitivity in Cancer (GDSC) project [28] (**Fig. 1a**). These high-throughput screens employed a 2 × 7 anchored dose design with partially measured dose-combination responses. To address the incompleteness of these matrices, we applied our DECREASE machine learning (ML) model [29] to predict complete 7 × 7 dose-combination matrices, after which widely-used synergy metrics (Bliss, Loewe, HSA and ZIP) were computed for each drug combination and cell line using the SynergyFinder 3.0 web-tool [15] (**Fig. 1b**). A sufficiently large set of multi-dose combination measurements is essential for reliable modelling and quantification of true synergistic and antagonistic effects in tissue-specific combination experiments.

The predicted synergy scores for 2,025 drug combination across 125 cancer cell lines were next used to establish reference null distributions for each tissue type and synergy metric (**Fig. 1b**, right panel). These reference distributions serve as null hypothesis models, capturing the "random" background variability in the tissue-specific combination measurements under the assumption that most of the interactions are additive (i.e., no significant interaction effect). This assumption is supported by large-scale combination screens showing that synergy is a rare event, occurring in ~5% of randomly-tested drug pairs [6, 10, 14]. Based on these reference distributions, empirical *p*-values can be derived for an observed synergy level (upper tail for synergy, lower tail for antagonism; see **Methods**), providing a measure of statistical significance in any combination screening assay. This statistical evaluation ensures that only combinations with sufficient

statistical evidence of synergy (or antagonism) are prioritized in the follow-up studies, reducing false positives and thereby decreasing the time and costs of the follow-up analyses.

Based on the empirical *p*-values (statistical significance) and the observed synergy scores (effect sizes), each drug combination in an experiment can be ranked within its respective tissue context (**Fig. 1c**). combinations with small *p*-values and high synergy scores are classified as the top synergistic hits, whereas those with significant negative scores are identified as the top antagonistic hits. Integrating statistical significance with effect size prioritizes the most reliable combinations for further mechanistic validation, analogous to differential gene expression analyses that jointly consider both fold changes and adjusted significance levels (volcano plots; **Fig. 1c**, right panel). Such dual-ranking approach facilitates the discovery of significant drug combinations that are likely to exhibit pre-clinically meaningful therapeutic effects when co-administered together in a specific cellular context.

Overall, this computational pipeline provides a scalable framework with reference distributions for statistical assessment of synergistic and antagonistic combination effects in cell-based viability assays, without requiring additional large-scale combination measurements across cell lines and concentrations. By integrating ML-based predictions, statistical evaluation, and dual-ranking of the combinations, our approach addresses the current statistical limitations of drug combination screening and improves the reproducibility of synergy detection across laboratories.

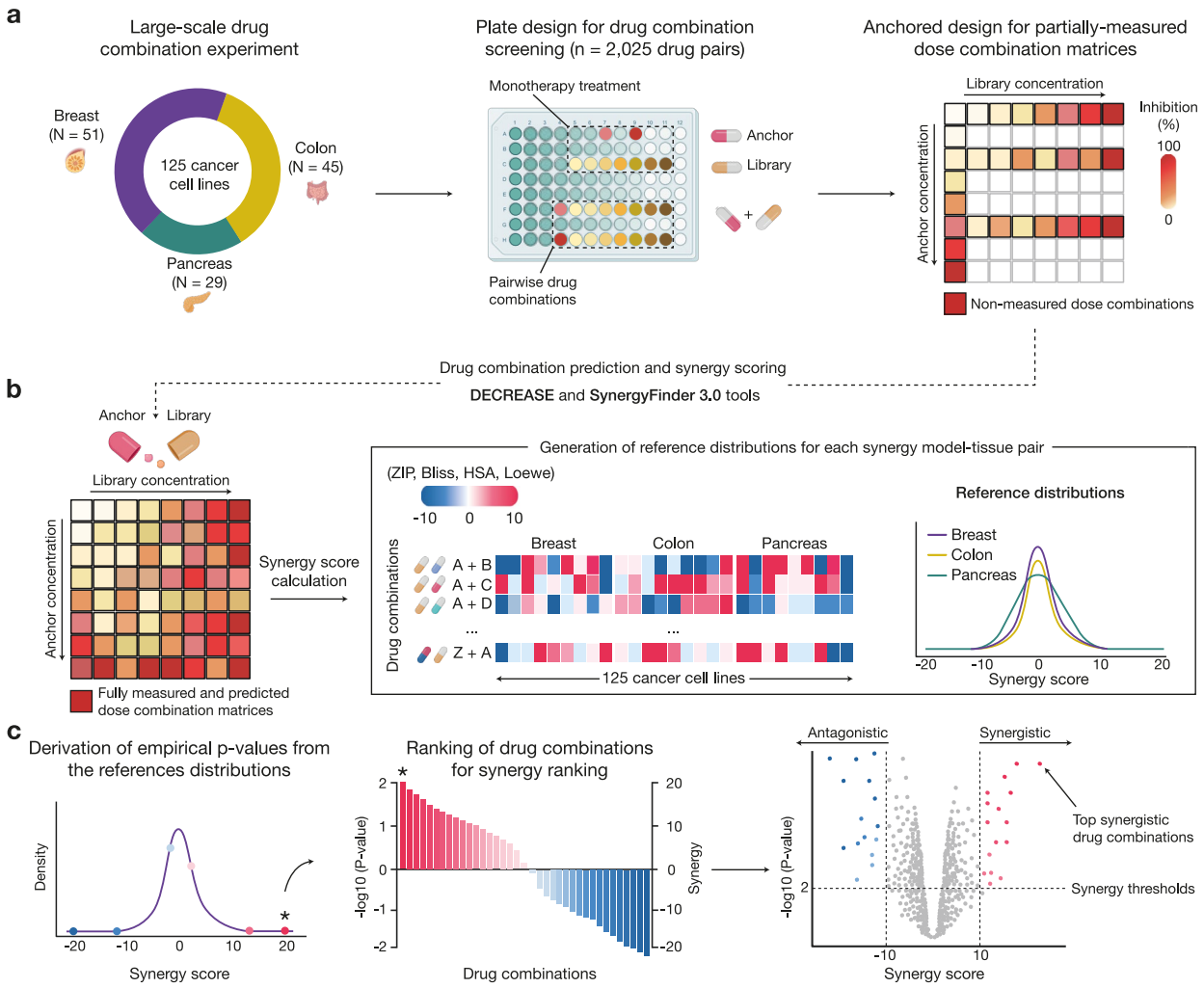

Figure 1. **A computational framework for the identification of statistically significant synergistic and antagonistic anticancer drug combinations.** (**a**) The Jaaks et al. 2 x 7 "anchored" dose-response drug combination design was used to evaluate *n*=2,025 drug pairs in *N*=125 cancer cell lines, resulting in partially-measured dose-combination matrices. (**b**) *Left:* Based on this large-scale dataset, the DECREASE machine learning model was used to predict the remaining, non-measured combination responses, enabling the subsequent computation of synergy metrics from complete 7 x 7 dose-response matrices using the SynergyFinder 3.0 web-tool. *Right*: reference distributions for the selected synergy metrics were generated across different tissues to derive empirical *p*-value, providing a measure of statistical significance of observed combination effects in new studies. (**c**) In applications of the reference distributions, the newly-tested drug combinations are ranked based on their synergy scores (effect size) and empirical *p*-values (statistical significance), with the top-ranked combinations identified as either synergistic or antagonistic hits.

Tissue-specific landscapes of synergistic and antagonistic combination effects

We next examined the distribution of synergy scores and their statistical significance using the tissue-specific reference distributions, calculated based on the 125 cancer cell lines and 2,025 drug pairs from the Jaaks et al. dataset (**Fig. 2**). This systematic statistical evaluation discovered novel synergistic and antagonistic interactions, enabled by completion of the full dose-combination matrices through the machine learning predictions (**Fig. 1**).

We first visualized the landscape of ZIP synergy scores across the drug combinations and cell lines in breast (N = 51), colon (N = 45), and pancreatic (N = 29) cancers. The analysis revealed distinct patterns of both synergy and antagonism stratified by drug combinations and cell line characteristics, including tissue of origin, point mutations, and biological pathways (**Fig. 2a**; **Suppl. File 1**). For instance, we found a distinct synergistic cluster of mostly pancreatic cancer cells (the black box), in which predominantly molecularly-targeted compounds were combined. In general, the cell lines did not cluster solely based on their tissue of origin or key point mutations, highlighting the cell context-specific heterogeneity in drug combination responses across the cell lines within and between the various tissue types. However, when analyzed within each tissue, or using different synergy metrics, notable differences emerged (**Suppl. Fig. 1**,**2**). Specifically, with the HSA metric, the combination landscape became inflated toward synergy, reflecting an inherent metric bias that positively skews HSA distributions and therefore affects synergy detection. Analyses with the Loewe metric resulted in a high proportion of non-evaluable combinations. Correlation analysis between the synergy metrics demonstrated relatively similar properties between ZIP and Bliss metrics (**Suppl. Fig. 3**; **Suppl. Table 1**). Based on these results, we selected ZIP as a balanced metric for subsequent synergy assessment; however, the statistical approach is broadly applicable to any of the existing or emerging synergy metrics.

To further investigate tissue-specific effects, we performed principal component analysis (PCA) on ZIP profiles, which revealed a clear tissue-specific separation of the cell lines (**Fig. 2b**), consistent with prior reports showing that tissue of origin shapes drug combination responses [13,14]. We therefore analyzed the reference null distributions of the ZIP synergy metric separately in each tissue type (**Fig. 2c**; **Suppl. Fig. 4**). The distributions exhibited modest shifts between the tissues, suggesting differences in overall synergy levels by cancer type. The ZIP reference distributions were relatively symmetric and distributed around zero, yet non-normally distributed (**Table 1**), indicating the need for non-parametric statistical assessment of tissue-specific significance. Bliss and ZIP metrics behaved rather similarly, whereas Loewe and HSA produced positively biased reference distributions (**Suppl. Fig. 5**). These reference null distributions form the basis for evaluating the statistical significance of an observed synergy in any combination screen, using a given synergy metric within a specific cancer type. The resulting p-value distributions showed an upper-tail enrichment (**Fig. 2d**; $p \leq 0.01$), consistent with synergy being a rare yet detectable event. Considering both the effect sizes and empirical significance is therefore essential to distinguish true interactions from additive background for follow-up studies.

Table 1. Distributional characteristics of the ZIP reference null distributions for the three tissue types.

Tissue	n	Mean	Median	Min	Max	SD	IQR	K-S test
Breast	62,322	-1.130	-1.110	-54.0	27.5	3.73	[-3.29, 1.08]	$p < 0.001$
Colon	28,029	-0.878	-0.825	-33.4	20.0	3.80	[-3.05, 1.36]	$p < 0.001$
Pancreas	19,252	-0.122	-0.110	-24.9	25.6	3.94	[-2.44, 2.22]	$p < 0.001$

n, the number of drug combinations evaluated across the cancer cell lines; SD, standard deviation; IQR, interquartile range; KS, Kolmogorov-Smirnov normality test. *Note*: small *p*-values indicate deviation from the normal distribution, due to large sample size and slightly heavier tails than in normal distribution. The empirical *p*-value calculation does not require normally distributed synergy scores.

To identify the strongest combination effects within each tissue, we ranked the drug pairs by their average ZIP score across the cell lines (**Fig. 2e**; **Suppl. File 2**). In breast cancer (n = 1,300 unique pairs), top synergistic combinations included Navitoclax with Tozasertib, Alisertib, ZM447439 and Paclitaxel. In colon cancer (n = 625), the highest-ranking pairs were Linsitinib with Sapitinib, Afatinib or Navitoclax, and AZD7762 with Camptothecin. In pancreatic cancer (n = 676), MK-2206 + SCH772984 emerged as the top synergistic hit, followed by Taselisib + Trametinib, Trametinib + MK-2206, and Paclitaxel + Navitoclax, with compounds appearing as either anchors or libraries. Similar conclusions were drawn for the antagonistic combinations. Using relatively stringent thresholds for effect size (ZIP ≥ 10 for synergy; ZIP ≤ −10 for antagonism) and empirical significance ($p \leq 0.01$), we identified a small subset of robust interaction effects (**Fig. 2f**), underscoring their rarity and tissue context-specificity. The fraction of significant synergistic or antagonistic pairs remained less or equal to 1%, as expected at this *p*-value threshold with the additional requirement for the ZIP cutoff. These cutoffs can be freely adjusted depending on the screening application, allowing researchers to balance sensitivity and specificity.

Together, these analyses show how the synergistic landscapes and reference distributions derived from large-scale data and complete combination matrices provide a systematic framework for making statistically robust conclusions about drug combination synergy or antagonism. This statistical approach further enables the detection of tissue-specific synergistic combinations in future studies using the pre-computed reference distributions from the Jaaks et al. dataset.

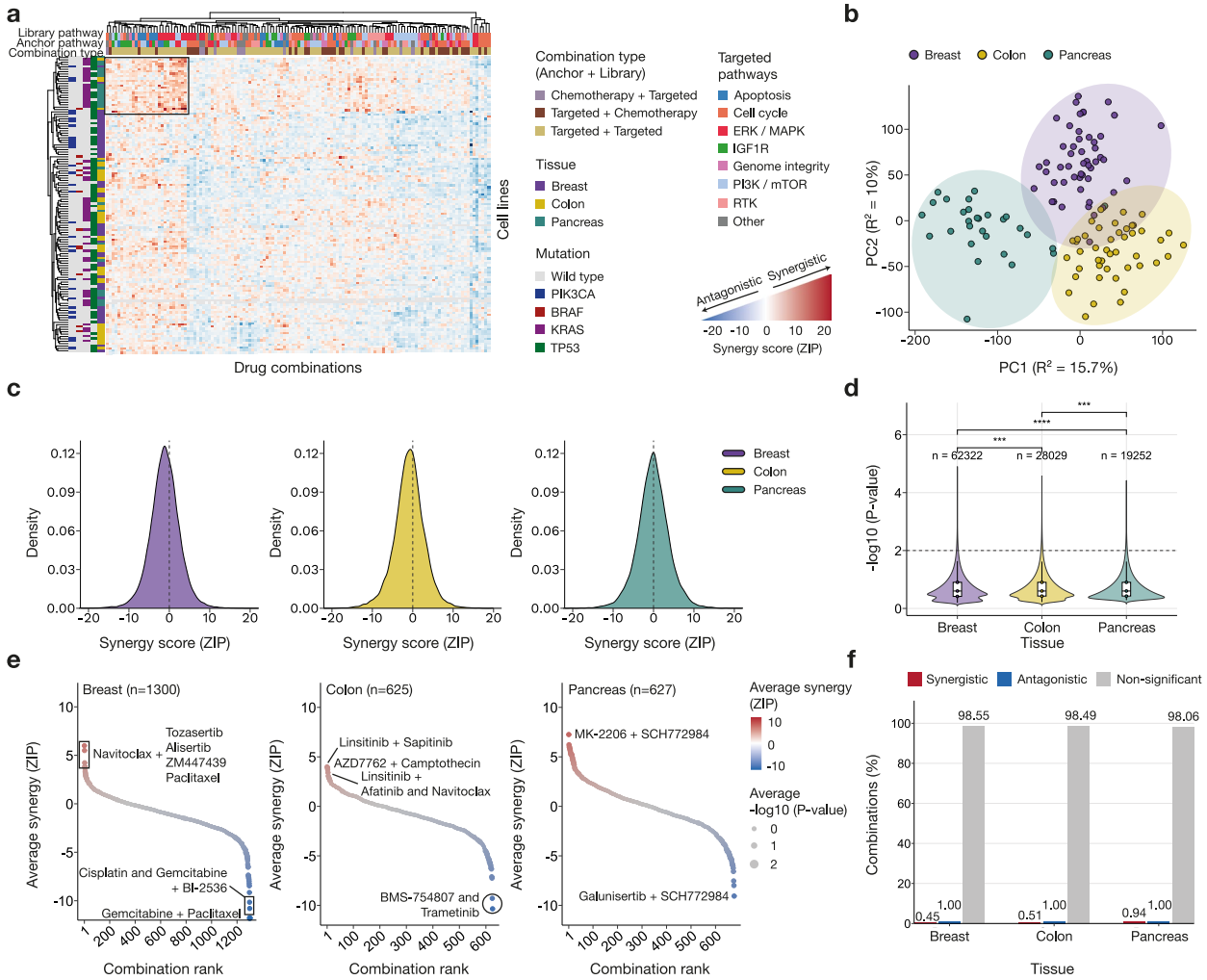

Figure 2. **Distribution of synergy scores across breast, colon, and pancreatic cancer cell lines after completing the full drug combination matrices.** (**a**) Heatmap of ZIP synergy scores for 125 cell lines and 2,025 drug pairs from the Jaaks et al. dataset, clustered by hierarchical clustering (complete linkage) using a custom Minkowski distance function. For visualization and cross-tissue comparison, combinations with >20% missing values were excluded, and only those drug pairs in which both anchor and library pathways were present in each tissue were retained (N=125, n=132). See **Suppl. Fig. 2** for full tissue-specific heatmaps. Colors indicate ZIP scores, with annotations for tissue of origin, key mutations, drug categories, and biological target pathways. (**b**) Principal component analysis (PCA) of the ZIP scores across all drug pairs and cell lines (the colored points). (**c**) Reference (null hypothesis) distributions of the ZIP scores across the three cancer tissues. The dotted horizontal line dashed marks zero ZIP synergy, corresponding to the additive baseline against which synergy is evaluated (synergy and antagonism). (**d**) Violin distributions of log-transformed *p*-values across the tissue types. The central dot indicates the median and the bars correspond to the interquartile range (IQR). The dotted horizontal line marks the selected significance cutoff of $p \leq 0.01$. Statistical significance was assessed using Wilcoxon rank-sum tests. ***$p < 0.001$, ****$p < 0.0001$. (**e**) Ranking of drug combinations by their average ZIP synergy across cell lines within each cancer type. Each point corresponds to a unique drug pair, with point size indicating the average p-value. Top-significant combinations are labelled (both synergists and antagonists). (**f**) Proportion of synergistic, antagonistic, and non-significant drug combinations based on ZIP synergy scores and empirical p-values, where synergy corresponds to ZIP ≥ 10 ($p \leq 0.01$) and antagonism to ZIP ≤ –10 ($p \leq 0.01$).

Identification of novel tissue-specific drug combinations and co-targeted pathways

We next statistically evaluated recurrent combination effects and their associated pathway targets across the three tissue types. To identify statistically significant combinations, we applied the relatively stringent thresholds for both effect size and significance (synergistic: ZIP ≥ 10, $p \leq 0.01$; antagonistic: ZIP ≤ –10, $p \leq 0.01$). This approach minimized false positive detections and enabled direct comparison with the synergy detections previously reported by Jaaks et al.

In breast cancer cell lines, the most frequently synergistic anchor drugs were Navitoclax (n = 78, N = 29), AZD7762 (n = 23, N = 16), and Linsitinib (n = 20, N = 14), often paired with library compounds such as Gemcitabine and Alisertib (**Fig. 3a**; **Suppl. File 3**) (n, number of significant instances; N, number of cell lines). Navitoclax, an inhibitor of the anti-apoptotic BCL-2 family, showed strong synergy with the Aurora kinase (AURKA) inhibitors Tozasertib (n = 11) and Alisertib (n = 10) (**Suppl. Fig. 6**), suggesting a potential apoptotic-mitotic target interaction in breast cancer. Among the colon cancer cell lines, Linsitinib (n = 19, N = 11), MK-2206 (n = 14, N = 8), and AZD7762 (n = 11, N = 9) emerged as the most frequently synergistic anchors, particularly when paired with DNA-damaging agents and PI3K/mTOR pathway inhibitors (**Fig. 3a**). In pancreatic cancer, Navitoclax emerged again as the top synergistic anchor (n = 30, N = 17), most notably in combination with the ERK1/ERK2 inhibitor SCH772984 and with Gemcitabine (**Suppl. Fig. 6**). The HuP-T4 cell line consistently exhibited high synergy, with OSI-027 + Trametinib and SCH772984 + Taselisib ranking among the strongest combinations, highlighting the potential benefit of co-targeting ERK/MAPK and PI3K/mTOR signaling in this tissue context. The strongest antagonistic interactions involved Palbociclib with Gemcitabine in breast cancer, suggesting that cell cycle inhibition may counteract genotoxic chemotherapy efficacy; SB216763 combined with Taselisib or BMS-754807 in colon cancer, pointing to suppressive effects from co-targeting WNT signaling alongside IGF1R or PI3K/mTOR pathways; and Galunisertib or LGK974 with SCH772984 in pancreatic cancer, suggesting potential suppression through co-inhibition of RTK/WNT and ERK/MAPK signaling.

To investigate the added value of using empirical p-values, we compared the synergistic hits identified by our approach to those reported by Jaaks et al., based on their ΔIC50 and ΔEmax metrics [13] (**Fig. 3b; Suppl. File 4**). Even under the stringent statistical cutoffs, our approach identified 24 additional synergistic combinations in breast cancer, 20 in colon cancer, and 13 in pancreatic cancer cell lines (**Suppl. File 5**). Notably, four common drug pairs demonstrated significant synergy across all three tissues (**Fig. 3c**), each involving the selective pan-Akt inhibitor MK-2206. These combinations occurred either in combination with Linsitinib and Trametinib, or with MK-2206 as the anchor paired with Trametinib or SCH772984, underscoring a pan-cancer synergistic effect from co-inhibition of PI3K/AKT/mTOR and ERK/MAPK signaling. Overall, molecularly targeted combinations dominated the significant synergies across tissue types, consistent with the observations made by Jaaks et al. [13].

To elucidate the molecular mechanisms driving combination synergy, we conducted pathway-level analyses stratified by anchor and library drugs across the three tissues (**Fig. 3d**; **Suppl. File 6**). In breast cancer, synergistic responses were predominantly associated with apoptosis, cell cycle progression, and DNA replication, with additional contributions from epigenetic and

cytoskeletal regulation. Colon cancer exhibited a more heterogeneous profile, with apoptotic and cell-cycle programs represented, but accompanied by signaling dependencies through IGF1R and WNT signaling. Pancreatic cancer stood out with synergism achieved mainly through PI3K/mTOR and ERK/MAPK signaling pathways, defining a kinase-driven synergy landscape.

The PI3K/mTOR pathway consistently emerged as a central target of synergy across the three cancer types. Highly synergistic combinations within this pathway led to highest synergies, particularly evident for the HuP-T4 pancreatic cell line (**Fig. 3e**). Pathway-level profiling of synergistic combinations identified a conserved set of recurrent processes across tissues, converging on cell survival and proliferative control, with IGF1R and WNT emerging as common drivers (**Fig. 3f**). In addition to the shared programs, tissue-specific signatures were evident; chromatin histone acetylation in breast cancer and ERK/MAPK signaling in pancreatic cancer. The latter was most apparent in HuP-T4, which consistently exhibited strong synergy (**Suppl. Fig. 7**). Antagonistic interactions in breast cancer were uniquely associated with co-targeting of p53 alongside cell-cycle and receptor tyrosine kinase (RTK) inhibition, whereas in colon and pancreatic models the WNT-pathway blockade frequently served as the backbone of antagonistic multi-target regimens (**Suppl. Fig. 8**). Overall, while synergistic responses converge on cell survival and proliferation programs, they are modulated by tissue-specific signaling, reflecting distinct oncogenic wiring and highlighting opportunities for context-specific therapy.

Together, these results demonstrate how our statistical framework enables rigorous identification of synergistic and antagonistic combinations that could otherwise be overlooked due to variability or incomplete experimental data. By integrating effect size with statistical significance, our method provides a robust foundation for the reliable discovery of biologically meaningful interactions in drug combination studies.

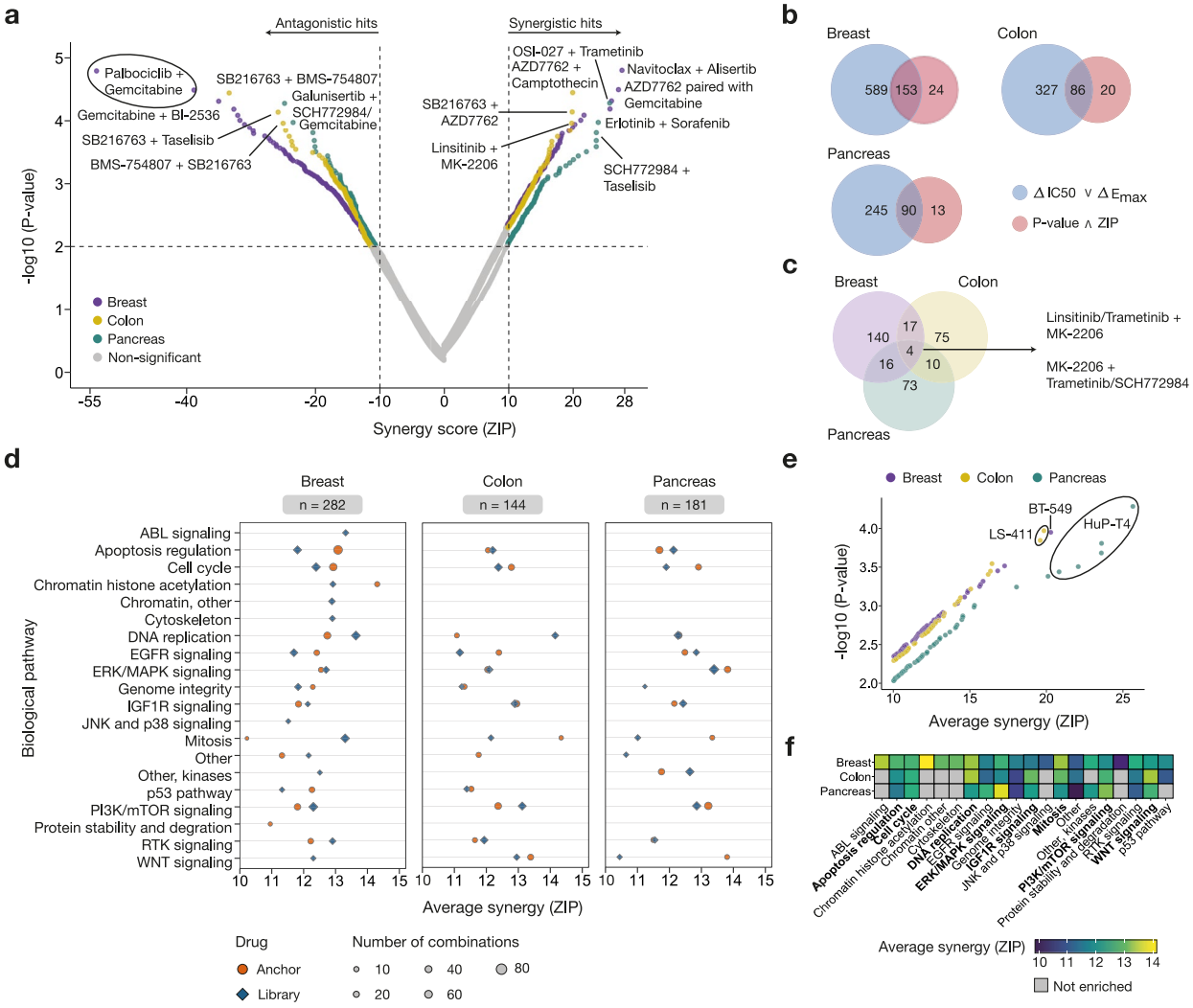

Figure 3. **Identification of significant drug combinations and target pathways.** (**a**) Volcano plots of ZIP synergy scores and empirical *p*-values for breast, colon, and pancreatic cancer cell lines. Each point corresponds to a cell line-drug pair. The key synergistic and antagonistic drug combinations are highlighted for each tissue, defined as empirical $p \leq 0.01$ and ZIP ≥ 10 or ZIP ≤ -10, respectively. Dashed lines mark the significance threshold and effect-size cutoff. (**b**) Number of synergistic drug combinations identified based on *p*-values and ZIP scores versus Jaaks et al. detections (△IC50 or △Emax). (**c**) Overlap of highly synergistic drug combinations identified across breast, colon, and pancreatic cancer cell lines (Breast: n = 177; Colon: n = 106, Pancreas: n = 103). Among the tested combinations, only four pairs were shared across the three tissues, each involving targeted agents. (**d**) Biological pathway enrichment analysis of the targets of synergistic drug combinations, stratified by anchor and library roles across the three tissues. The *x*-axis indicates the average ZIP synergy score across all the cell lines and combinations. (**e**) Synergistic drug combinations targeting the commonly enriched PI3K/mTOR pathway in breast, colon, and pancreatic cancers. Each point represents a unique drug pair tested in one or more cell lines, stratified and colored by the tissue of origin. The three cell lines that consistently ranked this pathway as the top hit are annotated. (**f**) Top 20 pathways with the highest average synergy across breast, colon, and pancreatic cancer cell lines. Pathways highlighted in bold represent those commonly observed across multiple cancer types, while grey denotes pathways not enriched or present in the particular tissue.

An application of the pre-computed reference distributions to an external dataset

To demonstrate the applicability of the reference distributions pre-computed in the Jaaks et al. dataset, we applied the approach to the 7 × 7 drug-dose combination matrix dataset of Bashi et al., which consisted of 109 pre-selected combinations [14]. Restricting the analysis to the same tissue types as those evaluated by Jaaks et al., we compared our statistical synergy assessment with a bootstrap-based null distribution and empirical *p*-value calculation (**Fig. 4a**).

The distribution of ZIP synergy scores in the Bashi et al. dataset displayed much heavier tails, with both extreme synergistic and antagonistic combinations, compared to the synergy distribution observed in the Jaaks et al. dataset for the matched tissue types (**Fig. 4b**, top panels). This was expected, as the 109 prioritized drug combinations in the Bashi et al. screen originated mainly from the AstraZeneca portfolio, and the library of 37 unique compounds covering diverse targets and mechanisms of action, including agents with evidenced potential for broad activity in pan-tumor panels and for clinical development. This is in contrast with the Jaaks et al. drug combination library, which was selected without any prior knowledge of potential synergy or antagonism, hence representing a more unbiased and close to random reference distribution. In all three tissue types, the Bashi et al. combinations showed statistical enrichment of strong synergistic and antagonistic effects (**Suppl. Table 2**), clearly visible in the tails of the cumulative distribution plots (**Fig. 4b**, bottom panels). Such heavy-tailed distributions cannot therefore be used as reference null distributions, even for this dataset, unless the significant synergistic and antagonistic combinations are first identified and removed.

We next subsampled the Bashi et al. breast cancer dataset to mimic the sample sizes of a typical drug combination experiment (**Fig. 4c**). When the number of cell lines and drug combinations was halved, the bootstrap null distributions began to diverge from the original dataset (**Fig. 4c**, subsample 2). This suggests that smaller datasets are no longer sufficiently representative of the true distribution, rendering the bootstrap procedure unreliable in smaller-scale combinatorial screens. We further evaluated the impact of data subsampling on synergy detections using the Jaaks et al. reference distributions as well as the Bashi et al. bootstrap null distributions (**Fig. 4d**). With the Jaaks reference, 8.98% of the full Bashi combinations were classified as synergistic ($p \leq 0.01$), confirming the enrichment of significant combinations compared to the Jaaks dataset. The variability in the proportions of significant combinations in the Bashi et al. subsamples (ranging from 6.04% to 12.20%) was expected, reflecting differences in the specific cell lines and drug combinations randomly included in each subsample. In contrast, the bootstrap-based statistical approach underestimated the number of synergistic combinations, with the proportion of significant combinations declining from 1.91% to 0%. This highlights the increasing inaccuracy of bootstrap-based detections in smaller datasets and underscores the value of using large-scale reference distributions to maintain sensitivity in synergy detection.

Due to the unique design of the Bashi et al. compound library, several AstraZeneca (AZ) compounds appeared among the top synergistic combinations, with the overall synergy landscape skewed toward positive interactions. Using our approach, we identified Mcl-1 inhibitor AZD5991 as a prominent synergistic hit across all tissues, most frequently paired with the Bcl-xL

inhibitor AZ-3202 (**Fig. 4e; Suppl. Fig. 9; and Suppl. File 7**). In addition, several DNA damage response (DDR)–targeting combinations emerged among the most synergistic hits. Specifically, the Chk1/Chk2 inhibitor Prexasertib displayed significant synergistic interactions when combined either with the Wee1 inhibitor AZD1775 or the topoisomerase I inhibitor SN-38. Similarly, the Chk1 inhibitor SRA737 showed synergistic interaction with Gemcitabine and SN-38, underscoring the therapeutic potential of targeting complementary DDR pathways to enhance cytotoxic responses. In contrast, several drug pairs were consistently identified among the strongest antagonistic interactions. Notably, the ATM inhibitor AZD0156 combined with the PARP inhibitor Olaparib emerged as a top antagonistic pair in both breast and colon cancer cell lines, highlighting recurrent efficacy suppression within the same DDR pathway. Antagonism commonly arose also from combinations converging on survival and cell cycle pathways, such as PI3K–mTOR inhibitors paired with CDK4/6 or apoptotic regulators. These findings suggest that targeting parallel survival mechanisms can sometimes blunt therapeutic activity rather than enhance it.

These results demonstrate how the well-powered null distributions derived based on the Jaaks et al. dataset can be applied to new drug combination screens and cell lines from the same tissues to guarantee accurate statistical evaluation. This avoids underestimation of true synergistic effects, even in smaller-scale settings, where the bootstrap procedures become increasingly unreliable.

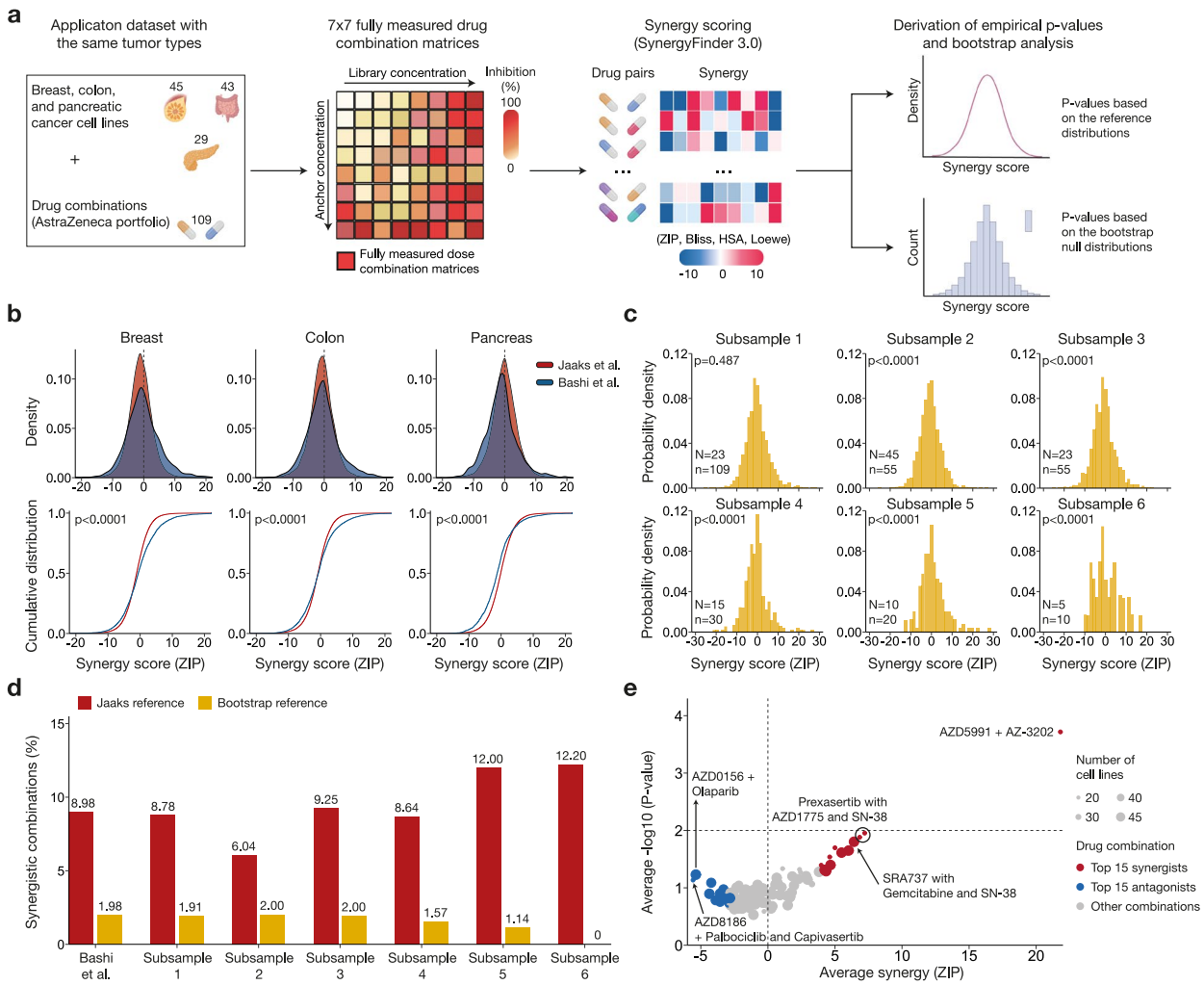

Figure 4. **Application of the reference distributions to an external drug combination dataset.** (**a**) The Bashi et al. 7 x 7 dose combination dataset was processed to include the same tissues tested as in Jaaks et al, enabling comparison of synergy detection with reference distributions and bootstrap-based analysis. (**b**) Comparison of the ZIP synergy score distributions between the Jaaks et al. and Bashi et al. datasets for each tissue type. *Top*: Probability density distributions of the ZIP synergy scores. *Bottom*: Empirical cumulative distributions of the ZIP scores, highlighting differences in the shape and range of the two datasets. Statistical significance was evaluated with a two-sample Kolmogorov-Smirnov test. (**c**) The bootstrap null distributions obtained by subsampling the full breast cancer dataset of the Bashi et al. (N = 45, n = 109). Each empirical null distribution was generated from 1,000 bootstrap resamples. Differences between the full and subsampled distributions were assessed using the Kolmogorov–Smirnov test. (**d**) Identification of statistically significant synergies in the Bashi et al. breast cancer cell line dataset based on empirical p-values ($p \leq 0.01$) using two null distributions: the Jaaks et al. reference (red) and the bootstrap reference (gold), each calculated based on 1000 bootstrap resamples per subsample. Bars represent the proportion of statistically significant synergistic combinations in the full Bashi et al. dataset and in six progressively smaller random subsamples, each containing approximately half the number of cell lines and drug combinations than the previous one. (**e**) Volcano plot of average ZIP scores against the average p-values in the breast cancer dataset. Each point represents a unique drug combination, with point size proportional to the number of cell lines tested. The dashed vertical line indicates the non-interaction threshold (ZIP = 0), and the dashed horizontal line denotes the significance cutoff of p = 0.01.

Discussion

Drug combination synergy is a relatively simple concept, where two or more drugs when used in combination result in greater than additive effects, compared to using the drugs individually as monotherapies. The complexity originates from the diverse biological mechanisms underlying synergistic interactions, as well as from the variety of metrics used to quantify and interpret combination effects [22,23,30]. To simplify and standardize this process, we introduced a statistical framework to identify robust synergistic and antagonistic drug combinations, building on two established platforms for drug combination prediction and synergy scoring: DECREASE [29] and SynergyFinder [31]. Leveraging partial dose–response matrices from Jaaks et al. [13], the combined use of these two methods enabled the pre-computation of reference distributions from complete 7×7 combination matrices across 2,025 drug pairs and 125 cancer cell lines. Regardless of the synergy metric applied, assessing combination effects at multiple doses is critical for defining synergy [23], as single-concentration designs can easily overlook synergistic or antagonistic interactions. Therefore, these reference distributions of close to random synergy scores provide a statistically robust and biologically justified means for evaluating the significance of observed drug interactions through empirical *p*-values. Our data-driven statistical approach enables a standardized definition of synergistic and antagonistic drug pairs in new screens. Importantly, this statistical evaluation enhances the discovery of truly synergistic drug combinations, thereby facilitating a faster and more reliable transition from preclinical to clinical investigation through improved robustness, statistical rigor, and reproducibility.

Even with a relatively stringent cutoff of $p \leq 0.01$, we identified 24 additional synergistic combinations in breast cancer, 20 in colon cancer, and 13 in pancreatic cancer compared to the original findings from Jaaks et al. [13], underscoring the added value of incorporating empirical *p*-values into synergy detection. However, equally important is the removal of false positive findings using the statistical synergy evaluation, since false detections will lead to wasted resources in follow-up experiments. The selected cutoffs provide rather conservative detections, as indicated by less than 2% of significant combinations in the Jaaks et al. dataset. Indeed, our approach reduces the number of false positives, while allowing end-users to adjust significance cutoffs according on the intended application (i.e., drug discovery applications may use less stringent cutoffs compared to confirmation assays). Applying the pre-computed reference distributions from Jaaks et al. to the fully-measured 7×7 pan-cancer dataset of Bashi et al. [14], we illustrated the broader applicability of our statistical framework, particularly in smaller-scale experiments where bootstrapping and other statistical procedures become unreliable. Given that drug combination screening is constrained by cost and time, and often restricted to only a few dozen pairs tested in small sets of cell lines and dose levels, the ability to obtain statistically rigorous results under such small data conditions provides a clear value for drug combination discovery.

To quantify potential synergistic effects, researchers commonly rely on established synergy metrics such as Bliss, Loewe, ZIP or HSA. As these models were developed based on different assumptions regarding drug interactions, they may lead to divergent classifications of synergism, additivity, and antagonism. Beyond selection of the synergy metric, researchers must also pre-define the cutoff threshold for synergy detection. Although *ad-hoc* synergy cutoffs, such as ZIP > 10 [32], provide straightforward means of selecting combinations for follow-up investigation,

focusing solely on the effect size (the level of synergy) overlooks the statistical significance of the observed synergy relative to the null hypothesis of no interaction (i.e., how likely it would be to observe such synergy level simply by random experimental variation). Furthermore, we demonstrated that the null hypothesis reference distributions may differ between the synergy metrics and tissue types, rendering universal cutoffs inaccurate, and promoting inconsistency between studies. For instance, HSA exhibited a positive bias even in random combinations, questioning its suitability for statistical usage. Although the use of empirical *p*-values can partly correct for such biases (e.g., non-central reference distributions), we recommend using alternative metrics, such as ZIP or Bliss, which demonstrate more balanced properties.

The identified combinations highlighted the tissue-specific nature of synergistic multi-agent therapies, driven by cell survival and proliferative control through DNA damage response, apoptosis regulation, and PI3K/mTOR signaling, while also revealing distinct tissue-specific signatures such as chromatin acetylation in breast cancer and ERK/MAPK signaling in pancreatic cancer. Our pathway-level analyses revealed distinct patterns of target enrichment across the three tissues. Synergy in breast cancer was primarily associated with the co-inhibition of cell cycle regulation, chromatin modification, and apoptotic pathways, suggesting that targeting the core processes of proliferation and survival may be particularly effective in this context. In colon cancer, synergistic effects were enriched in cell cycle regulation alongside IGF1R and WNT signaling, pointing to unique vulnerabilities in these models. In pancreatic cancer, the strongest enrichment arose from combinations targeting the ERK/MAPK and PI3K/mTOR pathways, underscoring the central role of these signaling pathways in shaping response to therapy. Collectively, these results indicate that while cell cycle programs represent a common therapeutic target across tumor types, tissue-specific signaling dependencies modulate optimal strategies for combinatorial treatment.

Historically, the development of safe and clinically relevant drug combination strategies has relied on empirical testing [3]. High-throughput screening (HTS) in cancer cell line panels *in vitro* and *ex vivo,* has enabled more systematic evaluation of a large number of combinations, whether pre-selected from observational clinical trials or guided by biologically-based hypotheses [4,7,8,9]. However, previous findings from large-scale screens show that synergistic drug interactions are relatively rare (ca. 5% of all drug pairs), and highly dependent on the cellular context and tissue of origin [6,10,13,14]. This underscores the need for robust statistical evaluation to address the challenge of identifying relatively rare, truly synergistic and tissue-specific combinations. Our statistical approach, which integrates both effect sizes (observed synergy score) and statistical significance (empirical *p*-value) enables the use of application-specific cutoffs, moving away from universal thresholds (e.g., using 5% of the most extreme synergies). This framework provides a scalable means of establishing reference distributions based on large-scale drug combination datasets and for prioritizing drug pairs that show statistically significant interactions. Once established, these reference distributions can be applied to assess the significance of observed synergy levels in any drug combination experiment, regardless of their scale.

Open questions remain, such as how to extend statistical synergy analysis beyond the three tumor types examined by Jaaks et al [13]. Since the reference distributions showed only modest differences between the tissue types, one could combine data from all tissues to generate a proxy reference distribution for other cancer types. Furthermore, once large enough combination

screens from other tissues become available, the same pipeline can be applied to derive new tissue-specific reference distributions. It has been shown that synergistic combinations are dominated by molecularly-targeted drugs [13]. For simplicity, we pooled all the tissue-specific combinations regardless of their drug classes or target pathways. However, one could establish separate reference distributions for distinct drug or target classes, depending on the drug library used in a new study. Similar principle applies to dosing, where dose-adjusted reference values could be generated to match the specific concentration ranges of interest. Alternatively, DECREASE [29] and other machine learning methods [33] can extrapolate beyond the measured dose matrix to expand the concentration window. Finally, in studies where healthy (e.g. non-cancerous) cells are profiled with the same combinations, one could infer selective synergy observed in cancer cells, relative to the toxic effects on healthy cells [12], or even to define a therapeutic dosage window that best balances between efficacy and toxicity.

Given these wide possibilities, we expect this work will facilitate standardized discovery of truly synergistic combinations for further validation in patient-derived models, ultimately supporting the development of safe and effective personalized combination therapies for clinical applications. This is particularly relevant for diseases like cancers, where cellular context-specificity and inter-patient heterogeneity pose major challenges for one-size-fits-all therapies.

Materials and Methods

Drug combination screening data

Jaaks et al. [13] generated a large-scale drug combination dataset comprising 2,025 drug pairs tested across 125 cancer cell lines (51 breast, 45 colorectal, and 29 pancreatic). In this dataset, drug combinations were screened using a so-called 2 × 7 anchored design, in which only a subset of the full drug-dose combination matrix was experimentally measured (see **Fig. 1a**). Each screening plate included a single replicate of the combination dose-response measurements, five replicates of the anchor drug, and four replicates of the monotherapy (single-agent) treatments. Cell viability response to drug treatments was assessed with CellTiter-Glo 2.0 (CTG 2.0, Promega) assays following the transfer of cells into 1,536-well microplates.

The screens were conducted using the Genomics of Drug Sensitivity in Cancer (GDSC) platform [28], generating thousands of viability measurements per drug combination across all cell lines. **Table 1** summarizes the number of drug combinations evaluated across the cell lines. The number of combinations varied between the tissues, due to the variable number of anchors and libraries tested on each plate, and since some of the combinations were not evaluated in each cell line. This dataset provided a suitable large-scale resource of effectively random combinations for constructing reference distributions of synergy scores for each of the three tissues (breast, colon, and pancreatic cancer).

The GDSC platform and CTG 2.0 assays were also used to generate another large-scale dataset by Bashi et al. [14], consisting of fully-measured drug-dose combination matrices for 109 selected anticancer drug pairs from the AstraZeneca's oncology library evaluated across 755 pan-cancer cell lines using a full 7 × 7 dose-response matrix design. This dataset was used to apply and test

the empirical p-values derived for observed synergy scores, using the reference distributions estimated from the Jaaks et al. dataset. Among other tissues, the Bashi et al. cell lines included breast carcinoma (n = 45), colorectal carcinoma (n = 43), and pancreatic carcinoma (n = 29).

Drug combination data preprocessing

In the Jaaks et al. dataset [13], the 2 × 7 anchored drug combination dose-response data were extracted from each screening plate, along with the corresponding monotherapy measurements for both the low and high anchor doses of the first drug and the seven-point concentration series of the library compound (i.e., the second drug in the pair). To complete the monotherapy profiles for the anchored drug, the missing dose-response data were retrieved from other screening plates in which the same anchored drug had been tested as the library drug in the 2 × 7 combination design. The median of the replicate measurements was used to compute the final viability values for both anchored and library monotherapy treatments. In some cases, certain compounds in this dataset included one or two extra concentrations in the monotherapy screens beyond the high/low anchor concentrations. As a result, some matrices expanded to 8 × 7 or 9 × 7 formats, which were also incorporated into our analysis. For the fully measured 7 × 7 drug combination matrix dataset from Bashi et al [14], the drug-dose response viability data for each combination and cell line were directly extracted from the respective screening plates for synergy computation, without any additional processing or ML predictions.

Drug combination prediction and synergy quantification

To complete the partially-measured drug combination matrices in Jaaks et al. dataset [13], the 2 x 7 dose-response combination measurements were used as input for the DECREASE machine learning algorithm; algorithmic details and validation results are provided in the original study [29]. DECREASE successfully predicted the full set of 7 x 7 pairwise drug-dose combination response matrices across all 125 cancer cell lines. The predicted combination matrices were then processed using the SynergyFinder v3.0 [15] to quantify synergy and antagonism using the Bliss, highest single-agent (HSA), Loewe and ZIP models. For Bashi et al. [14], synergy scores were directly computed from the 7 x 7 drug combination matrices without requiring matrix prediction.

Calculation of empirical *p*-values

To calculate the empirical p-values for the synergy scores derived from the Jaaks et al. reference distributions, the scores were processed separately for each tissue type. The reference synergy scores were sorted, and the empirical p-value for an observed synergy score was computed as the fraction of reference scores equal to or greater than the observed value, normalized by the total number of reference scores for that tissue. A two-tailed evaluation was conducted to evaluate statistical significance of both synergistic effects (positive synergy scores) and antagonistic effects (negative synergy scores).

$$\text{Empirical p-value} = \begin{cases} \frac{\sum_{i=1}^{n} \mathbb{I}(\text{score}_i \geq \text{observed score})}{n} & \text{if observed score} \geq 0 \\ \frac{\sum_{i=1}^{n} \mathbb{I}(\text{score}_i \leq \text{observed score})}{n} & \text{if observed score} < 0 \end{cases} \quad \text{(Eq. 1)}$$

- n is the total number of synergy scores for the tissue type;
- $score_i$ is the i^{th}reference synergy score ranked from smallest to largest;
- $observed\ score$ is the synergy value to be evaluated against the reference distribution;
- $\boldsymbol{I}(\cdot)$ is the indicator function, which returns 1 if the condition is true, and 0 otherwise.

We note that empirical *p*-value calculation is a non-parametric statistical procedure (i.e., it does not require normally distributed data). To assess the normality of the tissue-specific reference distributions, we applied two complementary normality tests. The Kolmogorov-Smirnov test is a nonparametric test widely used for comparing continuous probability distributions. The Anderson-Darling nonparametric normality test was additionally used for its higher sensitivity to deviations in the tails of the distribution (i.e., synergy or antagonism), and its robustness to ties.

Generation of bootstrap null distributions

To obtain smaller-scale data matrices from the Bashi et al. dataset, which better mimic the sample sizes of a typical drug combination experiment, we randomly subsampled both its drug combinations and cell lines without replacement. More specifically, from the full Bashi et al. dataset **X**, we draw a subsample **X*** of size *N* x *D* independently with equal probability for any given cell line - drug combination pair. For each subsample **X***, we then performed bootstrap resampling with replacement to generate 1,000, 2,000, or 5,000 resamples of the same size (*N* x *D)*. To derive the bootstrap null distributions, we primarily used 1,000 bootstrap resamples, as results were highly similar to those obtained with 2,000 or 5,000 resamples. The resulting null distributions were compared with those derived from the full Bashi et al. dataset using the Kolmogorov–Smirnov test. The bootstrap *p*-values were computed the same way as the empirical *p*-values from the Jaaks et al. data reference distributions (**Eq. 1**). The generation of 1,000, 2,000 and 5,000 bootstrap samples required approximately 23 minutes, 47 minutes, and 2 hours per tissue, respectively, when executed on the Puhti high-performance computing at CSC.

Data and code availability

Jaaks et al. [13] large-scale drug combination dataset can be freely accessed at https://figshare.com/articles/dataset/Original_screen_All_tissues_raw_data_csv_zip/19141916?file=34010816. Bashi et al. [14] drug combination dataset can be freely accessed at https://figshare.com/articles/dataset/Results_recorded_for_each_well_in_7x7_matrix_experiments_for_all_screens/25266697?file=45451363.

Analysis code for the manuscript figures and direct application of the reference distributions is available in the following repository: https://github.com/dias-dio/defining-synergy

Acknowledgments

We thank the authors of Jaaks et al. and Bashi et al. articles for making their combination data publicly available. The authors thank the CSC – IT Center for Science, Finland, for providing the computational resources. Funding support: AI: Ida Montin Foundation grant. TA: Research Council of Finland (grants 340141, 344698, 367855); the Cancer Society of Finland, the Norwegian Cancer Society (grants 216104 and 273810), Norwegian Health Authority South-East (grants 2020026 and 2023105), the Sigrid Jusélius Foundation, and iCAN – Digital Precision Cancer Medicine Flagship (iCAN-MULTIDRUG). Some graphical elements of Figure 1 were created with the help of the BioRender software.

Disclosure and competing interests statement

The authors declare that they have no conflict of interest.

References

[1] Al-Lazikani, B., Banerji, U. & Workman, P. Combinatorial drug therapy for cancer in the post-genomic era. *Nat Biotechnol* **30**, 679–692 (2012). https://doi.org/10.1038/nbt.2284
[2] Boshuizen, J., & Peeper, D. S. (2020). Rational cancer treatment combinations: An urgent clinical need. Molecular Cell, 78(6), 1002–1018. https://doi.org/10.1016/j.molcel.2020.05.031
[3] Jin, H., Wang, L. & Bernards, R. Rational combinations of targeted cancer therapies: background, advances and challenges. *Nat Rev Drug Discov* **22**, 213–234 (2023). https://doi.org/10.1038/s41573-022-00615-z
[4] Mott, B., Eastman, R., Guha, R. *et al.* High-throughput matrix screening identifies synergistic and antagonistic antimalarial drug combinations. *Sci Rep* **5**, 13891 (2015). https://doi.org/10.1038/srep13891
[5] KalantarMotamedi, Y., Eastman, R.T., Guha, R. *et al.* A systematic and prospectively validated approach for identifying synergistic drug combinations against malaria. *Malar J* **17**, 160 (2018). https://doi.org/10.1186/s12936-018-2294-5
[6] Yilancioglu, K., Cokol, M. Design of high-order antibiotic combinations against *M. tuberculosis* by ranking and exclusion. *Sci Rep* **9**, 11876 (2019). https://doi.org/10.1038/s41598-019-48410-y
[7] Holbeck, S. L., Camalier, R., Crowell, J. A., Govindharajulu, J. P., Hollingshead, M., Anderson, L. W., Polley, E., Rubinstein, L., Srivastava, A., Wilsker, D., Collins, J. M., & Doroshow, J. H. (2017). The National Cancer Institute ALMANAC: A Comprehensive Screening Resource for the Detection of Anticancer Drug Pairs with Enhanced Therapeutic Activity. *Cancer Research*, *77*(13), 3564–3576. https://doi.org/10.1158/0008-5472.CAN-17-0489
[8] O'Neil, J., Benita, Y., Feldman, I., Chenard, M., Roberts, B., Liu, Y., Li, J., Kral, A., Lejnine, S., Loboda, A., Arthur, W., Cristescu, R., Haines, B. B., Winter, C., Zhang, T., Bloecher, A., & Shumway, S. D. (2016). An Unbiased Oncology Compound Screen to Identify Novel Combination Strategies. *Molecular Cancer Therapeutics*, *15*(6), 1155–1162. https://doi.org/10.1158/1535-7163.MCT-15-0843

[9] Flobak, Å., Niederdorfer, B., Nakstad, V.T. *et al.* A high-throughput drug combination screen of targeted small molecule inhibitors in cancer cell lines. *Sci Data* **6**, 237 (2019). https://doi.org/10.1038/s41597-019-0255-7
[10] L.A. Mathews Griner, R. Guha, P. Shinn, R.M. Young, J.M. Keller, D. Liu, I.S. Goldlust, A. Yasgar, C. McKnight, M.B. Boxer, D.Y. Duveau, J. Jiang, S. Michael, T. Mierzwa, W. Huang, M.J. Walsh, B.T. Mott, P. Patel, W. Leister, D.J. Maloney, C.A. Leclair, G. Rai, A. Jadhav, B.D. Peyser, C.P. Austin, S.E. Martin, A. Simeonov, M. Ferrer, L.M. Staudt, & C.J. Thomas, High-throughput combinatorial screening identifies drugs that cooperate with ibrutinib to kill activated B-cell–like diffuse large B-cell lymphoma cells. *Proc. Natl. Acad. Sci. U.S.A*. 111 (6) 2349-2354, https://doi.org/10.1073/pnas.1311846111 (2014).
[11] Julkunen, H., Cichonska, A., Gautam, P. et al. Leveraging multi-way interactions for systematic prediction of pre-clinical drug combination effects. *Nat Commun* **11**, 6136 (2020). https://doi.org/10.1038/s41467-020-19950-z
[12] Ianevski, A., Nader, K., Driva, K. *et al.* Single-cell transcriptomes identify patient-tailored therapies for selective co-inhibition of cancer clones. *Nat Commun* **15**, 8579 (2024). https://doi.org/10.1038/s41467-024-52980-5
[13] Jaaks, P., Coker, E.A., Vis, D.J. *et al.* Effective drug combinations in breast, colon and pancreatic cancer cells. *Nature* **603**, 166–173 (2022). https://doi.org/10.1038/s41586-022-04437-2
[14] Bashi, A. C., Coker, E. A., Bulusu, K. C., Jaaks, P., Crafter, C., Lightfoot, H., Milo, M., McCarten, K., Jenkins, D. F., van der Meer, D., Lynch, J. T., Barthorpe, S., Andersen, C. L., Barry, S. T., Beck, A., Cidado, J., Gordon, J. A., Hall, C., Hall, J., Mali, I., … Garnett, M. J. (2024). Large-scale Pan-cancer Cell Line Screening Identifies Actionable and Effective Drug Combinations. *Cancer Discovery*, *14*(5), 846–865. https://doi.org/10.1158/2159-8290.CD-23-0388
[15] Aleksandr Ianevski, Anil K Giri, Tero Aittokallio, SynergyFinder 3.0: an interactive analysis and consensus interpretation of multi-drug synergies across multiple samples, *Nucleic Acids Research*, 50, Issue W1, 5 July 2022, Pages W739–W743, https://doi.org/10.1093/nar/gkac382
[16] Giovanni Y. Di Veroli, Chiara Fornari, Dennis Wang, Séverine Mollard, Jo L. Bramhall, Frances M. Richards, Duncan I. Jodrell, Combenefit: an interactive platform for the analysis and visualization of drug combinations, *Bioinformatics*, Volume 32, Issue 18, September 2016, Pages 2866–2868, https://doi.org/10.1093/bioinformatics/btw230
[17] Bliss, C. I. (1939). The toxicity of poisons applied jointly. *Annals of Applied Biology, 26*(3), 585–615. https://doi.org/10.1111/j.1744-7348.1939.tb06990.x
[18] Loewe, S. (1953). The problem of synergism and antagonism of combined drugs Arzneimittelforschung 3: 285–290.
[19] Berenbaum, M. C. (1989). What is synergy? Pharmacological reviews, 41(2), 93-141.
[20] Gaddum, J. H. (1940). Pharmacology (pp. 378–383). Oxford University Press. https://www.jameslindlibrary.org/gaddum-jh-1940/
[21] Yadav, B., Wennerberg, K., Aittokallio, T., & Tang, J. (2015). Searching for Drug Synergy in Complex Dose-Response Landscapes Using an Interaction Potency Model. *Computational and structural biotechnology journal*, *13*, 504–513. https://doi.org/10.1016/j.csbj.2015.09.001
[22] Tang J, Wennerberg K and Aittokallio T (2015) What is synergy? The Saariselkä agreement revisited. *Front. Pharmacol*. 6:181. https://doi.org/10.3389/fphar.2015.00181

[23] Vlot, A. H. C., Aniceto, N., Menden, M. P., Ulrich-Merzenich, G., & Bender, A. (2019). Applying synergy metrics to combination screening data: agreements, disagreements and pitfalls. *Drug discovery today*, *24*(12), 2286–2298. https://doi.org/10.1016/j.drudis.2019.09.002
[24] Nair, N.U., Greninger, P., Zhang, X. *et al.* A landscape of response to drug combinations in non-small cell lung cancer. *Nat Commun* **14**, 3830 (2023). https://doi.org/10.1038/s41467-023-39528-9
[25] Vis, D. J., Jaaks, P., Aben, N., Coker, E. A., Barthorpe, S., Beck, A., Hall, C., Hall, J., Lightfoot, H., Lleshi, E., Mironenko, T., Richardson, L., Tolley, C., Garnett, M. J., & Wessels, L. F. A. (2024). A pan-cancer screen identifies drug combination benefit in cancer cell lines at the individual and population level. *Cell Reports. Medicine*, *5*(8), 101687. https://doi.org/10.1016/j.xcrm.2024.101687
[26] Ocana, A., Amir, E., Yeung, C., Seruga, B., & Tannock, I. F. (2012). How valid are claims for synergy in published clinical studies?. *Annals of oncology: official journal of the European Society for Medical Oncology*, *23*(8), 2161–2166. https://doi.org/10.1093/annonc/mdr608
[27] Makariadou, E., Wang, X., Hein, N., Deresa, N. W., Mutambanengwe, K., Verbist, B., & Thas, O. (2025). Synergy detection: A practical guide to statistical assessment of potential drug combinations. *Pharmaceutical statistics*, *24*(1), e2383. https://doi.org/10.1002/pst.2383
[28] Iorio, F., Knijnenburg, T. A., Vis, D. J., Bignell, G. R., Menden, M. P., Schubert, M., Aben, N., Gonçalves, E., Barthorpe, S., Lightfoot, H., Cokelaer, T., Greninger, P., van Dyk, E., Chang, H., de Silva, H., Heyn, H., Deng, X., Egan, R. K., Liu, Q., Mironenko, T., … Garnett, M. J. (2016). A Landscape of Pharmacogenomic Interactions in Cancer. *Cell*, *166*(3), 740–754. https://doi.org/10.1016/j.cell.2016.06.017
[29] Ianevski, A., Giri, A.K., Gautam, P. et al. Prediction of drug combination effects with a minimal set of experiments. *Nat Mach Intell* **1**, 568–577 (2019). https://doi.org/10.1038/s42256-019-0122-4
[30] Fitzgerald, J., Schoeberl, B., Nielsen, U. *et al.* Systems biology and combination therapy in the quest for clinical efficacy. *Nat Chem Biol* **2**, 458–466 (2006). https://doi.org/10.1038/nchembio817
[31] Athanasiadis, P., Ianevski, A., Skånland, S.S., Aittokallio, T. (2022). Computational Pipeline for Rational Drug Combination Screening in Patient-Derived Cells. In: Carugo, O., Eisenhaber, F. (eds) Data Mining Techniques for the Life Sciences. Methods in Molecular Biology, vol 2449. Humana, New York, NY. https://doi.org/10.1007/978-1-0716-2095-3_14
[32] Aleksandr Ianevski, Anil K Giri, Tero Aittokallio, SynergyFinder 2.0: visual analytics of multi-drug combination synergies, *Nucleic Acids Research*, Volume 48, Issue W1, 02 July 2020, Pages W488–W493, https://doi.org/10.1093/nar/gkaa216
[33] Huusari, R., Wang, T., Szedmak, S. *et al.* Predicting drug combination response surfaces. *npj Drug Discov.* **2**, 2 (2025). https://doi.org/10.1038/s44386-024-00004-z